Frequency Analysis of the In-Plane Rotating Hub-Beam System Considering Effects of the Hub

Jun-wei Chen, Le-tong Ma, Bo Zhang(✉), and Han Ding

State Key Laboratory of Mechanical System and Vibration, School of Mechanical Engineering, Shanghai Jiao Tong University, Shanghai 200240, China
cjwbuaa@163.com, m835527262@126.com, {b_zhang,hding}@sjtu.edu.cn

Abstract. In this paper, the in-plane rotating hub-beam system is mainly investigated considering effects of the hub. By applying the extended Hamilton's principle and the Galerkin method, the governing equation of motion of the hub-beam system is derived. The hub-beam rotary inertia ratio is investigated to reveal its effect on the frequency characteristics of the rotating hub-beam system. Through the frequency analysis, it is shown that the natural frequencies of different orders vary between those of the clamped and the pinned boundary conditions at the connecting point between the hub and the beam. Finally the figure of connecting rigidity is plotted to show the variation.

Keywords: Hub-beam system · Dynamic stiffening · Rigid-flexible coupling

1 Introduction

The rotating beam is a fundamental element in mechanical engineering. Along with the high precision required in applications, such as rotating blades, antennas, robot arms, spinning space structures, etc., the dynamic characteristics of the rotating beam are of great importance for the mechanical design and evaluation due to dynamic stiffening.

Therefore many researchers have studied this phenomenon since it was pointed out in 1987 [1]. Yoo et al. [2-4] applied the Kane's method to model a rotating cantilever beam by assumed mode method. Utilizing the same discretization method, Hong & Liu developed first order approximating coupling (FOAC) model by the principle of virtual work [5,6]. In these papers, the dynamic stiffening due to the rotation of the single beam itself was mainly concerned and reasonable explanations about the natural frequencies were given and justified. Usually, it is regarded that it is clamped at the connecting point between the hub and the beam. This is reasonable when the rotary inertia of the hub is large. However, as the experimental and analytical work in [7-10] showed, the actual boundary condition is between the pinned and clamped boundary conditions at the connecting point, depending on the hub property.

This is meaningful for some engineering applications where a rotating beam is driven by a light hub. In such applications, the flexible connection between the hub and the beam has impact on the natural frequencies and dynamic response of the beam. So in this paper, considering the effect of dynamic stiffening, the effect of the

H. Liu et al. (Eds.): ICIRA 2015, Part I, LNAI 9244, pp. 15–23, 2015.
DOI: 10.1007/978-3-319-22879-2_2

hub property to the natural frequency of the rotating beam is investigated. First, the dynamic model of the rotating hub-beam system was developed by employing the extended Hamilton's principle and the Galerkin method. Then the governing equation for frequency analysis was formulated, and the variation of natural frequencies due to different values of rotary inertia of the hub was studied. Finally, conclusions are given.

2 Modeling

In this section, the rotating hub-beam system considering geometric nonlinearity is modelled based on the linear elasticity law and the Euler-Bernoulli model. Fig. 1 illustrates the configuration of the system. The rigid hub and the flexible beam are driven by the externally applied torque $M(t)$ at the hub center O in the global Cartesian coordinate system O-X_0Y_0. The body Cartesian coordinate system O-x_by_b, fixed to point O, is initially aligned to O-X_0Y_0.

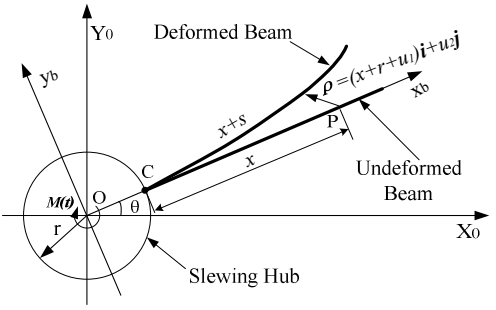

Fig. 1. Configuration of the rotating hub-beam system

2.1 Description of Deformation

As showed in Fig. 1, the displacement vector of a generic point P can be represented in O-x_by_b as,

$$\boldsymbol{\rho} = (x + r + u_1)\boldsymbol{i} + u_2\boldsymbol{j} \tag{1}$$

where $\boldsymbol{i}, \boldsymbol{j}$ are unit vectors of O-x_by_b, and u_1, u_2 are the respective deformation along each unit vector. Introduce $\boldsymbol{A}$ to denote the transforming matrix from O-x_by_b to O-X_0Y_0 as,

$$\boldsymbol{A} = \begin{bmatrix} cos\theta & -sin\theta \\ sin\theta & cos\theta \end{bmatrix} \tag{2}$$

The displacement vector in O-X_0Y_0 can be represented as follows.

$$\boldsymbol{r}=\boldsymbol{A}\boldsymbol{\rho} \tag{3}$$

Differentiating $\boldsymbol{r}$ yields,

$$\dot{\boldsymbol{r}} = \dot{\theta}\boldsymbol{A}\tilde{\boldsymbol{I}}\boldsymbol{\rho} + \boldsymbol{A}\dot{\boldsymbol{\rho}} \tag{4}$$

where

$$\tilde{\boldsymbol{I}} = \begin{bmatrix} 0 & -1 \\ 1 & 0 \end{bmatrix}, \qquad \dot{\boldsymbol{\rho}} = \begin{bmatrix} \dot{u}_1 \\ \dot{u}_2 \end{bmatrix}$$

Considering geometric nonlinearity, the axial displacements of Eulerian description is utilized instead of u_1, which is represented as in [3]

$$s = u_1 + \frac{1}{2}\int_0^x \left[\left(\frac{\partial u_2}{\partial x}\right)^2\right] dx \tag{5}$$

Then by the Galerkin method, one obtains.

$$s(x,t) = \boldsymbol{\phi}_1^T(x)\boldsymbol{q}_1(t) \tag{6}$$

$$u_2(x,t) = \boldsymbol{\phi}_2^T(x)\boldsymbol{q}_2(t) \tag{7}$$

where $\boldsymbol{\phi}_i = [\phi_{i1}\ \phi_{i2}\ \cdots]^T$ and $\boldsymbol{q}_i = [q_{i1}\ q_{i2}\ \cdots]^T$. Generally, any compact set of functions satisfying geometric boundary conditions can be applied as the spatial functions $\boldsymbol{\phi}_i$ [11]. In this study, the orthonormal modes of a clamped-free beam [12] are utilized.

2.2 Potential Energy

The strain energy of the beam due to the axial inertia force and the transverse blending is expressed as in [3],

$$U = \frac{1}{2}\int_0^l EA\left(\frac{\partial s}{\partial x}\right)^2 dx + \frac{1}{2}\int_0^l EI\left(\frac{\partial^2 u_2}{\partial x^2}\right)^2 dx \tag{8}$$

where E is the Young's modulus, A is the cross-section area of the beam, l the length of the beam, I the second area moment of inertia of the cross section.

2.3 Kinetic Energy

The kinetic energy of the system consists of those of the hub and the beam, i.e.,

$$T = \frac{1}{2}J_h\dot{\theta}^2 + \frac{1}{2}\int_0^l \rho A\dot{\boldsymbol{r}}\cdot\dot{\boldsymbol{r}}dx \tag{9}$$

where J_h is the hub rotary inertia, and ρ mass density of the beam.

2.4 Governing Equations

Assuming $x + r \gg u_1$ and neglecting higher-order nonlinear terms, the governing equations of motion are formulated by the extended Hamilton's principle as,

$$\sum_{i=1}^{\mu_2}\left[\int_0^l \rho A(x+r)\phi_{2i}dx\right]\ddot{q}_{2i} + \left[J_h + \int_0^l \rho A(x+r)^2 dx\right]\ddot{\theta} = M(t) \tag{10}$$

$$\sum_{i=1}^{\mu_2}\ddot{q}_{2i}\int_0^l \rho A\phi_{2i}\phi_{2j}dx + \ddot{\theta}\int_0^l \rho A(x+r)\phi_{2j}dx + 2\dot{\theta}\sum_{i=1}^{\mu_1}\int_0^l \rho A\phi_{1i}\phi_{2j}dx\,\dot{q}_{1i} -$$

$$\dot{\theta}^2\sum_{i=1}^{\mu_2} q_{2i}\left[\int_0^l \rho A\phi_{2i}\phi_{2j}dx + \frac{1}{2}\int_0^l \rho A(x^2-l^2)\frac{\partial\phi_{2i}}{\partial x}\frac{\partial\phi_{2j}}{\partial x}dx + r\int_0^l \rho A(x-\right.$$

$$\left. l)\frac{\partial\phi_{2i}}{\partial x}\frac{\partial\phi_{2j}}{\partial x}dx\right] + \sum_{i=1}^{\mu_2} q_{2i}\int_0^l EI\frac{\partial^2\phi_{2i}}{\partial x^2}\frac{\partial^2\phi_{2j}}{\partial x^2}dx = 0 \qquad (j = 1,2,\ldots\mu_2) \tag{11}$$

where μ_1 and μ_2 are the number of generalized coordinates for s and u_2, respectively. Obviously, Eqs. (10) and (11) are coupled due to the Coriolis effect. Since the stretching natural frequencies are much greater than the bending ones [13], it is sensible to ignore the coupling terms within the range concerned in the following.

For simplicity, introduce the following dimensionless variables.

$$\delta = \frac{r}{l}, \quad \beta = \frac{J_h}{\rho A l^3}, \quad \xi = \frac{x}{l}, \quad \tau = \sqrt{T_0}t, \quad \gamma(\tau) = \theta(t), \quad \dot{\gamma}(\tau) = \frac{\dot{\theta}(t)}{\sqrt{T_0}},$$

$$p(\tau) = \frac{q_2(t)}{l}, \quad \psi_2(\xi) = \phi_2(x), \quad \eta(\tau) = \frac{l}{EI}M(t), \quad T_0 = \frac{EI}{\rho A l^4}.$$

Then Eqs. (10) and (11) are simplified as

$$\begin{bmatrix}\sigma & \boldsymbol{C}^T\\ \boldsymbol{C} & \mathbf{M}\end{bmatrix}\begin{bmatrix}\ddot{\gamma}\\ \ddot{\boldsymbol{p}}\end{bmatrix} + \left(\begin{bmatrix}0 & 0\\ 0 & \mathbf{K}^s\end{bmatrix} - \dot{\gamma}^2\begin{bmatrix}0 & 0\\ 0 & \Delta\mathbf{K}\end{bmatrix}\right)\begin{bmatrix}\gamma\\ \boldsymbol{p}\end{bmatrix} = \begin{bmatrix}\eta(\tau)\\ 0\end{bmatrix} \tag{12}$$

where

$$\sigma = \beta + \frac{1}{3}(1 + 3\delta + 3\delta^2)$$

$$\boldsymbol{C} = \int_0^1 (\xi + \delta)\boldsymbol{\psi}_2 d\xi$$

$$\mathbf{M} = \int_0^1 \boldsymbol{\psi}_2\boldsymbol{\psi}_2^T d\xi$$

$$\mathbf{K}^s = \int_0^1 \frac{\partial^2\boldsymbol{\psi}_2}{\partial\xi^2}\frac{\partial^2\boldsymbol{\psi}_2^T}{\partial\xi^2}d\xi$$

$$\Delta\mathbf{K} = \mathbf{M} + \delta\mathbf{K}^{d1} + \frac{1}{2}\mathbf{K}^{d2}$$

$$\mathbf{K}^{d1} = \int_0^1 (\xi - 1) \frac{\partial \boldsymbol{\psi}_2}{\partial \xi} \frac{\partial \boldsymbol{\psi}_2^T}{\partial \xi} d\xi$$

$$\mathbf{K}^{d2} = \int_0^1 (\xi^2 - 1) \frac{\partial \boldsymbol{\psi}_2}{\partial \xi} \frac{\partial \boldsymbol{\psi}_2^T}{\partial \xi} d\xi$$

3 Frequency Analysis

In Eq. (12), rigid rotating motion and in-plane bending vibration are highly coupled, and hub radius ratio δ can affect the stiffness matrix obviously. Since this parameter has been studied a lot [14,11,15], rotary inertia of the hub is mainly focused on.

For frequency analysis, set $\eta(\tau)$ to zero. Let ω denote the dimensionless natural frequency, then it obtains,

$$\left[\omega^2 \left(\mathbf{M} - \frac{1}{\sigma} \boldsymbol{C} \cdot \boldsymbol{C}^T\right) - (\mathbf{K}^s - \dot{\gamma}^2 \Delta \mathbf{K})\right] \boldsymbol{p} = 0 \tag{13}$$

The curved surfaces of the first two order dimensionless natural frequencies are demonstrated in Fig. 2. It is showed that ω tends to increase as $\dot{\gamma}$ gets larger due to the effect of dynamic stiffening, which has been verified by many researchers. Meanwhile, hub-beam ratio of rotary inertia β has great effect on the varying trends of ω. In Fig. 2, the black solid lines represent the natural frequencies under the clamped boundary condition at the hub end, and the black solid lines with dots represent those of the pinned boundary condition (though they are plotted at $\beta = 5$). At different values of the angular velocity, the natural frequency of each order of the hub-beam system varies between those of the pinned-free and the clamped-free boundary conditions. That is, ω approaches the natural frequency of the rotating beam under the pinned-free boundary condition when β is close to zero, and that of the rotating beam under the clamped-free boundary condition when β is close to infinity. The above phenomenon was tested through a physical experiment using a high speed camera in Ref. [7].

To further reveal and verify the above phenomenon, Fig. 3 is plotted to show the curved lines of ω vs. $\dot{\gamma}$. The black curved lines stand for the 1st order natural frequencies of different values of β, which clearly demonstrate the aforementioned changing rule in terms of ω about β. The same changing rule in terms of ω about β exists for other orders, so the corresponding curved lines are omitted. Besides, the blue curved line is plotted for comparison to represent the 2nd order natural frequency when β approximates to infinity. And the black asterisks and upper triangles represent the 1st and 2nd order dimensionless natural frequencies given in Ref. [3], respectively. Since the clamped-free boundary condition was applied in Ref. [3], its results agree with the curved lines of $\beta \to \infty$.

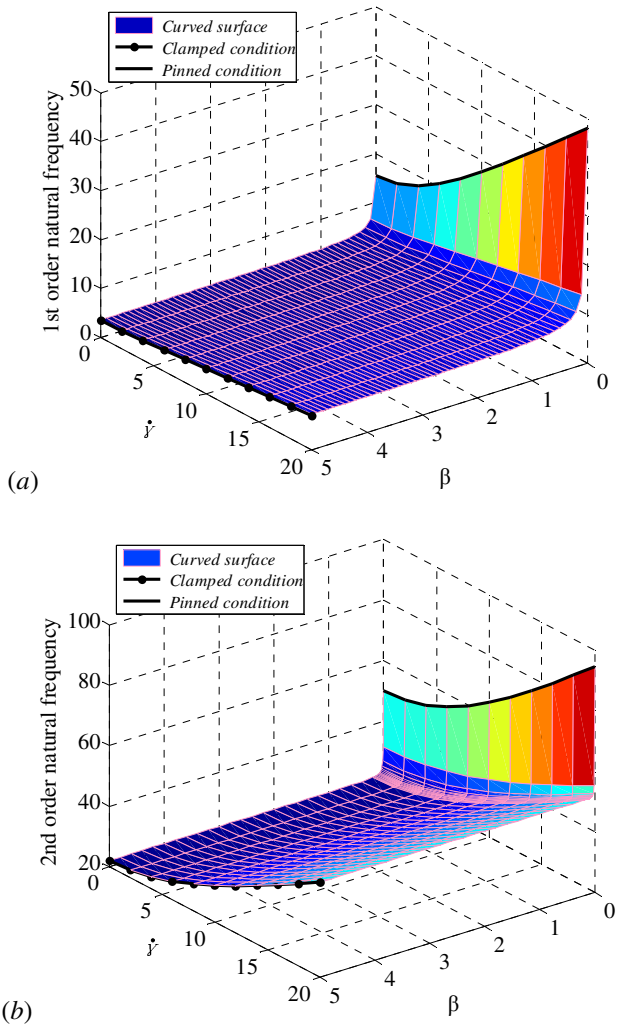

Fig. 2. Curved surfaces of ω in terms of β and $\dot{\gamma}$: (*a*) 1st order; (*b*) 2nd order

Fig. 4 shows the varying tendency of ω vs. β of different orders, where some specified points are compared with those in Ref. [8]. The corresponding results agree well. Besides, it can be observed that ω declines very fast when β is close to zero, and very slow after β passes 1. In other words, the greater β is, the less the decreasing rate is. So ω is more sensitive to β when β approaches zero.

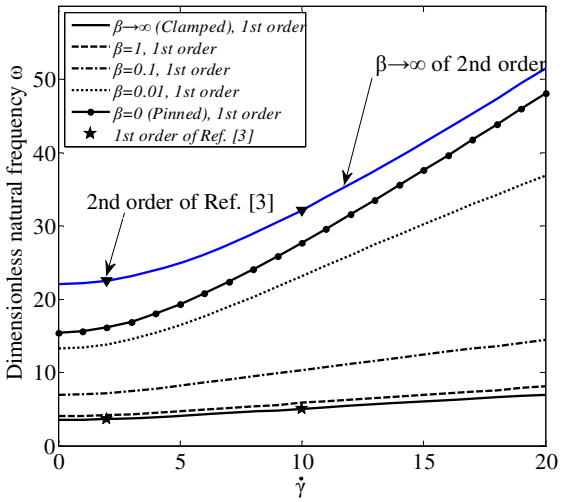

Fig. 3. ω vs. $\dot{\gamma}$ of different values of β

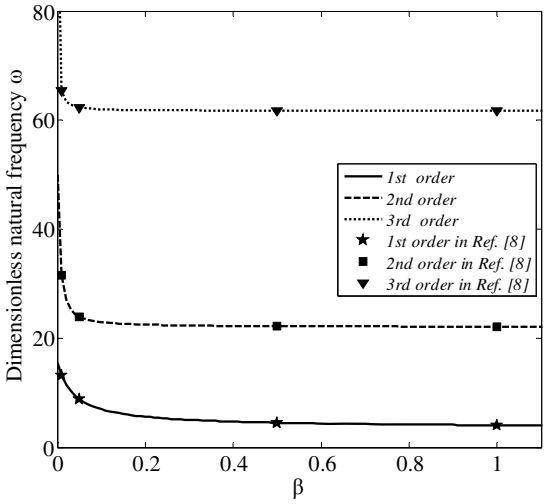

Fig. 4. ω vs. β of different orders

Based on the definition of the clamped and the pinned boundary conditions, it can be regarded that the connecting rigidity between the hub and the beam is infinity in the case of the clamped-free boundary condition, and zero in the case of the pinned-free boundary condition. As a result, the range of β can be divided into three regions, as shown in Fig. 5. Region I is the region with very low connecting rigidity, region II is the highly rigid-flexible coupling region with intermediate connecting rigidity, and region

III is the region with high connecting rigidity. Such division is clear to understand the rigid-flexible coupling between the hub and the beam, and is meaningful for engineering practice.

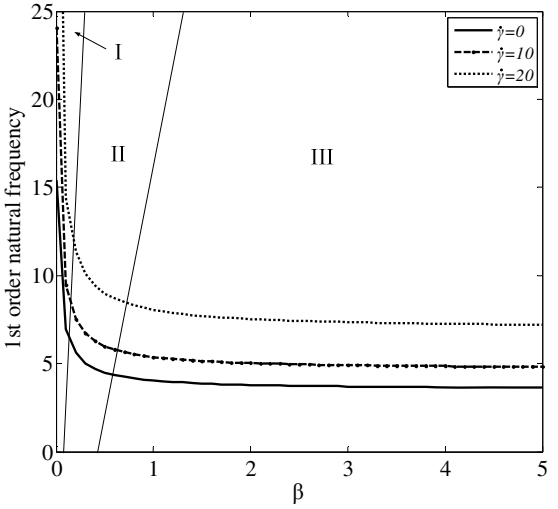

Fig. 5. Division of the range of β

4 Conclusions

In this paper, the effect of the hub on the in-plane rotating hub-beam system is investigated. By applying the extended Hamilton's principle and the Galerkin method, the governing equation of motion of the hub-beam system is derived. Frequency analysis shows that the natural frequencies of different orders vary between those of the clamped and the pinned boundary conditions at the connecting point between the hub and the beam. Zero value of the hub inertia leads to the pinned boundary condition, and the infinity value of the hub inertia leads to the clamped boundary condition. Due to this flexibility, the phenomenon is meaningful for engineering design.

Acknowledgements. This work was supported by the National Natural Science Foundation of China under grant 51375312, for which the authors are grateful.

References

1. Kane, T.R., Ryan, R.R., Banerjee, A.K.: Dynamics of a cantilever beam attached to a moving base. Journal of Guidance, Control, and Dynamics **10**(2), 139–151 (1987)
2. Seo, S., Yoo, H.H.: Dynamic analysis of flexible beams undergoing overall motion employing linear strain measures. Aiaa J. **40**(2), 319–326 (2002)

3. Yoo, H.H., Shin, S.H.: Vibration analysis of rotating cantilever beams. Journal of Sound and Vibration **212**(5), 807–808 (1998)
4. Yoo, H.H., Seo, S., Huh, K.: The effect of a concentrated mass on the modal characteristics of a rotating cantilever beam. Proceedings of the Institution of Mechanical Engineers, Part C: Journal of Mechanical Engineering Science **216**(2), 151–164 (2002). doi:10.1243/0954406021525098
5. Liu, J.Y., Hong, J.Z.: Dynamics of three-dimensional beams undergoing large overall motion. European Journal of Mechanics, A/Solids **23**(6), 1051–1068 (2004). doi:10.1016/j.euromechsol.2004.08.003
6. Liu, J.Y., Hong, J.Z.: Geometric stiffening effect on rigid-flexible coupling dynamics of an elastic beam. Journal of Sound and Vibration **278**(4–5), 1147–1162 (2004). doi:10.1016/j.jsv.2003.10.014
7. Low, K.H., Lau, M.W.S.: Experimental investigation of the boundary condition of slewing beams using a high-speed camera system. Mechanism and Machine Theory **30**(4), 629–643 (1995)
8. Low, K.H.: A note on the effect of hub inertia and payload on the vibration of a flexible slewing link. Journal of Sound and Vibration **204**(5), 823–828 (1997)
9. Bellezza, F., Lanari, L., Ulivi, G.: Exact modeling of the flexible slewing link. In: Proceedings of the 1990 IEEE International Conference on Robotics and Automation, pp. 734-739. Publ. by IEEE, Cincinnati
10. Morris, K.A., Taylor, K.J.: A Variational Calculus Approach to the Modelling of Flexible Manipulators. SIAM Review **38**(2), 294–305 (1996)
11. Zhu, T.L.: The vibrations of pre-twisted rotating Timoshenko beams by the Rayleigh-Ritz method. Computational Mechanics **47**(4), 395–408 (2011). doi:10.1007/s00466-010-0550-9
12. Blevins, R.D. (ed.): Formulas for natural frequency and mode shape. Krieger, Malabar, Fla (1979)
13. Yoo, H.H., Cho, J.E., Chung, J.: Modal analysis and shape optimization of rotating cantilever beams. Journal of Sound and Vibration **290**(1–2), 223–241 (2006). doi:10.1016/j.jsv.2005.03.014
14. Hamdan, M.N., Al-Bedoor, B.O.: Non-linear free vibrations of a rotating flexible arm. Journal of Sound and Vibration **242**(5), 839–853 (2001). doi:10.1006/jsvi.2000.3387
15. Lin, S.C., Hsiao, K.M.: Vibration analysis of a rotating Timoshenko beam. Journal of Sound and Vibration **240**(2), 303–322 (2001). doi:10.1006/jsvi.2000.3234